When heptane complex **2** is trapped by $PPh_3$ or $Et_3SiH$, the only slightly greater stabilization of the transition state by the incoming phosphine ligand in comparison to the stabilization provided by $Et_3SiH$ is consistent with an early transition state with very little Mn-P bond formation. This suggests that the transition state has very little associative character. With a dissociative transition state, the overwhelming component to $\Delta H_{-1}^{\ddagger}$ is loss of the Mn-heptane interaction in **2**. Thus, the value for $\Delta H_{-1}^{\ddagger}$ provides a lower bound of approximately 8 kcal/mol for the magnitude of this interaction. We had previously estimated the Mn-heptane interaction in **2** to be approximately 8-9 kcal/mol by comparison of activation enthalpies and enthalpies of reaction for the substitution of *cis*-cyclooctene and dibutyl sulfide from $CpMn(CO)_2L$ by phosphine and phosphite ligands.[10] Both previous estimates and the estimate reported here, although in good agreement with one another, are in error to the degree that a residual Mn-heptane interaction exists in the transition state. Rayner's studies on metal-hydrocarbon interactions clearly show them to be in the 10-kcal/mol range.[23] As a consequence, we believe that although the true Mn-heptane interaction may be somewhat greater than 8 kcal/mol, the difference is probably not substantial.

Finally, with the observation of a substantial Mn-heptane interaction in complex **2**, both the $\Delta H_{Mn-CO}$ and the $\Delta H_{-1}$ values reported here are smaller in magnitude than the corresponding gas-phase values. Thus, the gas-phase Mn-CO bond dissociation energy is then calculated to be 54.8 kcal/mol and the enthalpy of addition of $Et_3SiH$ to $CpMn(CO)_2$ is -28.1 kcal/mol.

**Acknowledgment.** We acknowledge the National Institutes of Health (Grant No. GM-42704) and the donors of the Petroleum Research Fund, administered by the American Chemical Society, for financial support of this research. D.M.H. acknowledges support from a U.S. Department of Education Fellowship Grant to the USC Chemistry Department. A.W.H. acknowledges partial support from an NSF-REU grant.

**Supplementary Material Available:** Listings of $k_{obsd}$ at different $[PPh_3]$ and $[Et_3SiH]$ for the reaction of $CpMn(CO)_2(H)(SiEt_3)$ with $PPh_3$ in heptane solution at 35, 50, 60, 70, and 80 °C (2 pages). Ordering information is given on any current masthead page.

(23) (a) Ishikawa, Y.; Brown, C. E.; Hackett, P. A.; Rayner, D. M. *Chem. Phys. Lett.* **1988**, *150*, 506-510. (b) Brown, C. E.; Ishikawa, Y.; Hackett, P. A.; Rayner, D. M. *J. Am. Chem. Soc.* **1990**, *112*, 2530-2536.

# Synthesis and Characterization of Trinuclear Iron(II) and Manganese(II) Carboxylate Complexes: Structural Trends in Low Valent Iron and Manganese Carboxylates

**R. Lynn Rardin, Peter Poganiuch, Avi Bino,[1] David P. Goldberg, William B. Tolman, Shuncheng Liu, and Stephen J. Lippard***

*Contribution from the Department of Chemistry, Massachusetts Institute of Technology, Cambridge, Massachusetts 02139.* *Received December 20, 1991*

**Abstract:** Reaction of $Fe(O_2CCH_3)_2$ or $Mn(O_2CCH_3)_2 \cdot 4H_2O$ with bidentate nitrogen donor ligands affords the trinuclear complexes $[M_3(O_2CCH_3)_6L_2]$ [M = Fe, L = BIPhMe (**1**); M = Mn, L = BiPhMe (**2**) or 1,10-phenanthroline (**3**)] in high yields. As judged from X-ray diffraction studies, these complexes adopt a novel linear structure, with one monodentate and two bidentate bridging carboxylates spanning each pair of metal atoms. Within this motif there are two geometric isomers that exist, designated "syn" or "anti" depending upon the orientation of the bidentate nitrogen donor ligands with respect to one another across the plane defined by the three metal atoms and the two monodentate bridging oxygen atoms. The bidentate and monodentate bridging modes are related by a carboxylate shift mechanism, proposed on the basis of observed variations in the interaction of the nonbridging, or dangling, oxygen atoms of the monodentate carboxylates with the terminal metal atoms. Such a carboxylate shift has recently been observed for the bridged dimetallic center in ribonucleotide reductase. Structural characterization of three isomers of compound **2** revealed a considerable degree of flexibility in the tricarboxylate-bridged dimetallic unit, with M···M distances ranging from 3.370 (3) to 3.715 (2) Å. From temperature-dependent magnetic susceptibility studies, compound **1** was found to be a ferromagnetically coupled triiron(II) complex with bridging oxygen atoms. A theoretical fit of the magnetic susceptibility data for **1** revealed the $J$ value for ferromagnetic exchange coupling between adjacent iron atoms to be in the range +5 to +10 $cm^{-1}$. Magnetic susceptibility results for **2** revealed more typical antiferromagnetic coupling, with $J = -2.8$ (1) $cm^{-1}$ for adjacent manganese atoms. The relevance of these results to the properties of carboxylate-bridged dimetallic iron and manganese centers in metalloproteins and the chemical reactivity of the complexes are briefly discussed.

## Introduction

Proteins containing non-heme polyiron or polymanganese oxo units in their active centers, including hemerythrin (Hr), ribonucleotide reductase (RR), methane monooxygenase (MMO), purple acid phosphatase (PAP), the water oxidizing center of photosystem II (PSII), and ferritin, have been the subject of considerable investigation.[2-16] For most of these proteins, redox chemistry is involved in the key functional steps, with the metals cycling among the +2, +3, and +4 oxidation states. Whereas

Scheme I

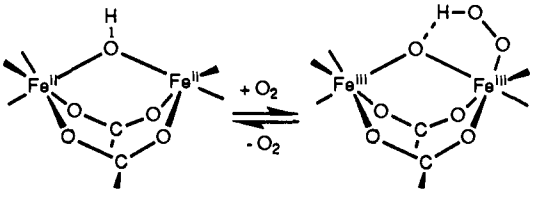


deoxyHr oxyHr

(1) Permanent address: Department of Inorganic and Analytical Chemistry, Hebrew University of Jerusalem, 91904 Jerusalem, Israel.
(2) Lippard, S. J. *Angew. Chem., Int. Ed. Engl.* **1988**, *27*, 344.
(3) Que, L., Jr.; True, A. E. *Prog. Inorg. Chem.* **1990**, *38*, 97.
(4) Kurtz, D. M., Jr. *Chem. Rev.* **1990**, *90*, 585.
(5) Vincent, J. B.; Olivier-Lilley, G. L.; Averill, B. A. *Chem. Rev.* **1990**, *90*, 1447.

0002-7863/92/1514-5240$03.00/0 

**Chart I**

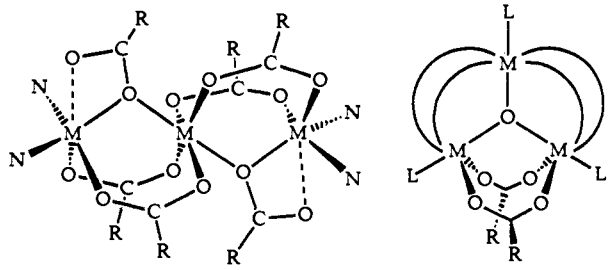

$[M_3(O_2CCH_3)_6L_2]$ $[M_3O(O_2CR)_6L_3]^{n+}$

basic carboxylate

considerable information is now available about the higher oxidation states of the polyiron and polymanganese oxo centers through the study of model compounds, much less is known about the reduced (+2) state.[2,3,7-10,13] In the case of Hr models,[17-19] for example, diiron(III) complexes have been synthesized that are excellent structural and spectroscopic mimics for metazidoHr, an inactive form of the protein.[20] Only a few divalent iron complexes have been synthesized as models[19,21-23] for the functionally more relevant diiron(II) deoxy form of the protein, however, none which binds dioxygen in the manner proposed for the protein (Scheme I).[6]

With the shift in focus from the preparation of models for the structural and physical properties of the metal centers in this class of proteins to the more difficult task of reproducing the functional chemistry, attention has turned to divalent iron and manganese. In the course of studying the reactions of Mn(II) and Fe(II) with biomimetic carboxylate and polyimidazole ligands, we have synthesized several new trinuclear complexes with a novel linear structure, $[M_3(O_2CCH_3)_6L_2]$ [M = Fe, L = BIPhMe[24] (**1**); M = Mn, L = BIPhMe (**2**) or phen[24] (**3**)]. The structures of these complexes (Chart I), together with that of geometrically related diiron(II) complex, $[Fe_2(O_2CCH)_4(BIPhMe)_2]$ (**4**),[22,23] reveal a new tricarboxylate-bridged motif for polyiron/manganese centers that appears thus far to be characteristic of the divalent oxidation state. Previously, the dominant structure in trinuclear iron- and manganese-carboxylate chemistry was the oxo-centered equilateral triangle of the basic carboxylates, $[M_3O(O_2CR)_6L_3]^{n+}$, $n$ = 0, 1 (Chart I). This type of complex was reported as early as 1865[25] and has been the subject of numerous studies since that time.[26]

In the present article, we describe the synthesis, geometry, physical properties, and a preliminary investigation of the reactivity of the new family of trinuclear carboxylates, some aspects of which were previously communicated in preliminary form for **1** and **2**.[27] Of particular interest are the variable geometries observed for these complexes, analysis of which has led to the concept of the carboxylate shift.[28] Interestingly, just such a shift has been recently discovered for the dimetallic center in ribonucleotide reductase.[29-31]

## Experimental Section

**Materials and General Methods.** Solvents and reagents were obtained from commercial sources and used as received, unless noted otherwise. The ligand 1,10-phenanthroline·$H_2O$ was purchased from Fluka Chemical Corp., Ronkonkoma, NY. BIPhMe was prepared by a literature method.[23] Elemental analyses were performed by Atlantic Microlab, Inc., Atlanta, GA. IR spectra were recorded for KBr discs of **1–3** on a Mattson Cygnus 100 Fourier transform spectrometer.

**Synthesis.** **$[Fe_3(O_2CCH_3)_6(BIPhMe)_2]$ (1).** A mixture of $Fe(O_2CCH_3)_2$ (1.85 g, 10.64 mmol) and BIPhMe (2.00 g, 7.08 mmol) was allowed to stir for 1 h in methanol (22 mL) under argon at 50 °C, affording a clear, pale green solution. The volume of the solution was reduced by 50% in vacuo, after which tetrahydrofuran vapor was diffused into the solution, yielding crystals of *anti*-**1**·2THF (2.77 g, 72% yield) suitable for X-ray diffraction studies after 1 week: FT-IR (KBr) 3126, 3107, 2974, 2967, 2871, 1597 ($\nu_{asym}$ $CO_2$), 1500, 1448, 1417 ($\nu_{sym}$ $CO_2$), 1372, 1306, 1285, 1142, 1068, 989, 895, 798, 762, 723, 704, 656, 645 $cm^{-1}$. Anal. Calcd for $C_{52}H_{70}Fe_3N_8O_{16}$: C, 50.75; H, 5.73; N, 9.10. Found: C, 50.83; H, 5.80; N, 9.40.

**$[Mn_3(O_2CCH_3)_6(BIPhMe)_2]$ (2).** A slurry of $Mn(O_2CCH_3)_2·4H_2O$ (0.13 g, 0.53 mmol) and BIPhMe (0.10 g, 0.35 mmol) in methanol (2 mL) was allowed to stir in air for 15 min, producing a clear, nearly colorless solution. Addition of diethyl ether yielded **2** as a beige solid (0.154 g, 81% yield). The solid was dried in vacuo prior to elemental analysis: FT-IR (KBr) 3130, 3047, 3030, 3004, 2962, 2930, 2831, 1597 ($\nu_{asym}$ $CO_2$), 1497, 1448, 1416 ($\nu_{sym}$ $CO_2$), 1338, 1281, 1174, 1155, 1138, 1089, 1068, 1018, 988, 895, 757, 721, 704, 672, 646 $cm^{-1}$. Anal. Calcd for $C_{44}H_{54}Mn_3N_8O_{14}$: C, 48.76; H, 5.02; N, 10.34. Found: C, 48.43; H, 4.97; N, 10.53.

Three isomers of **2** were crystallized and structurally characterized. They are designated *anti*-**2A**, *anti*-**2B**, and *syn*-**2** based on the disposition of the BIPhMe imidazole groups with respect to the best plane passing through the three metal atoms and the two monodentate carboxylate oxygen bridges. The A designation indicates the anti isomer where the central metal is located on a crystallographic inversion center; no such inversion center exists in the B form. X-ray quality crystals of *anti*-**2A**·$2CH_2Cl_2$ were obtained by slow evaporation of a methylene chloride solution of **2**. Crystals of *anti*-**2B** were obtained by slow evaporation of an ethanol/methanol solution of **2**, while suitable crystals of *syn*-**2**·$3CH_2Cl_2$ were obtained by vapor diffusion of diethyl ether into a methylene chloride solution of **2**.

**$[Mn_3(O_2CCH_3)_6(phen)_2]$ (3).** A solution of 1,10-phenanthroline·$H_2O$ (0.54 g, 2.72 mmol) in 20 mL of dimethylformamide (DMF) was added to a stirred solution of $Mn(O_2CCH_3)_2·4H_2O$ (1.00 g, 4.08 mmol) in 40 mL of DMF. A yellow solid began to precipitate as the ligand solution was added. The mixture was allowed to stir for 10 min and was then filtered, yielding a fine yellow solid that was washed with several aliquots of DMF, followed by several aliquots of acetone, and then diethyl ether. The solid was dried in vacuo to yield a pale yellow powder (1.00 g, 99% yield): FT-IR (KBr) 3059, 3016, 3002, 2997, 2930, 1582 ($\nu_{asym}$ $CO_2$), 1516, 1427 ($\nu_{sym}$ $CO_2$), 1420, 1345, 1338, 1222, 1149, 1140, 1102, 1048, 1016, 867, 849, 777, 729, 670, 659, 655, 639, 618 $cm^{-1}$. Anal. Calcd for $C_{36}H_{34}Mn_3N_4O_{12}$: C, 49.16; H, 3.90; N, 6.37. Found: C, 48.56; H, 3.90; N, 6.51.

Pale yellow crystals of **3** suitable for an X-ray diffraction study were obtained within hours by allowing low concentration DMF solutions of $Mn(O_2CCH_3)_2·4H_2O$ to react with 1,10-phenanthroline and letting the

(6) Sanders-Loehr, J. In *Iron Carriers and Iron Proteins*; Loehr, T. M., Ed.; VCH Publishers: New York, 1989; p 373.
(7) Wilkins, P. C.; Wilkins, R. G. *Coord. Chem. Rev.* **1987**, *79*, 195.
(8) Wieghardt, K. *Angew. Chem., Int. Ed. Engl.* **1989**, *28*, 1153.
(9) Vincent, J. B.; Christou, G. *Adv. Inorg. Chem. Radiochem.* **1989**, *33*, 197.
(10) Christou, G. *Acc. Chem. Res.* **1989**, *22*, 328.
(11) Brudvig, G. W.; Beck, W. F.; dePaula, J. C. *Annu. Rev. Biophys. Biophys. Chem.* **1989**, *18*, 25.
(12) Brudvig, G. W.; Crabtree, R. H. *Prog. Inorg. Chem.* **1989**, *37*, 99.
(13) Christou, G.; Vincent, J. B. *ACS Symp. Ser.* **1988**, *372*, 238.
(14) Brudvig, G. W. *ACS Symp. Ser.* **1988**, *372*, 221.
(15) Renger, G. *Angew. Chem., Int. Ed. Engl.* **1987**, *26*, 643.
(16) Cammack, R.; Chapman, A.; Lu, W.-P.; Karagouni, A.; Kelly, D. P. *FEBS Lett.* **1989**, *253*, 239.
(17) Armstrong, W. H.; Spool, A.; Papaefthymiou, G. C.; Frankel, R. B.; Lippard, S. J. *J. Am. Chem. Soc.* **1984**, *106*, 3653.
(18) Wieghardt, K.; Pohl, K.; Gebert, K. *Angew. Chem., Int. Ed. Engl.* **1983**, *22*, 727.
(19) Hartman, J. R.; Rardin, R. L.; Chaudhuri, P.; Pohl, K.; Wieghardt, K.; Nuber, B.; Weiss, J.; Papafthymiou, G. C.; Frankel, R. B.; Lippard, S. J. *J. Am. Chem. Soc.* **1987**, *109*, 7387.
(20) Sheriff, S.; Hendrickson, W. A.; Smith, J. L. *J. Mol. Biol.* **1987**, *197*, 273.
(21) Borovik, A. S.; Que, L., Jr. *J. Am. Chem. Soc.* **1988**, *110*, 2345.
(22) Tolman, W. B.; Bino, A.; Lippard, S. J. *J. Am. Chem. Soc.* **1989**, *111*, 8522.
(23) Tolman, W. B.; Liu, S.; Bentsen, J. G.; Lippard, S. J. *J. Am. Chem. Soc.* **1991**, *113*, 152.
(24) Ligand abbreviations: BIPhMe, 2,2′-bis(1-methylimidazolyl)-phenylmethoxymethane; phen, 1,10-phenanthroline; $H_2$saladhp, 2-(salicylideneamino)-1,3-dihydroxy-2-methylpropane; $Me_3$TACN, 1,4,7-trimethyl-1,4,7-triazacyclononane; bpy, 2,2′-bipyridine; salamp, bis(salicylideneamino)-2-methylphenolate(3−); bpmp, 2,6-[(bis(2-pyridylmethyl)amino)-methyl]-4-methylphenolate(1−); $H_2$salpn, *N,N′*-bis(salicylidene)propylenediamine; DMF, dimethylformamide.
(25) Schützenberger, M. P. *Bull. Soc. Chim. Fr.* **1865**, *4*, 86.
(26) Cannon, R. D.; White, R. P. *Prog. Inorg. Chem.* **1988**, *36*, 195.
(27) Rardin, R. L.; Bino, A.; Poganiuch, P.; Tolman, W. B.; Liu, S.; Lippard, S. J. *Angew. Chem., Int. Ed. Engl.* **1990**, *29*, 812.
(28) Rardin, R. L.; Tolman, W. B.; Lippard, S. J. *New J. Chem.* **1991**, *15*, 417.
(29) Nordlund, P.; Sjöberg, B.-M.; Eklund, H. *Nature* **1990**, *345*, 593.
(30) Atta, M.; Nordlund, P.; Åberg, A.; Eklund, H.; Fontecave, M. *J. Biol. Chem.*, submitted for publication.
(31) Nordlund, P., personal communication.

**Table I.** Experimental Details of the X-ray Diffraction Studies[a] of *anti*-$[Fe_3(O_2CCH_3)_6(BIPhMe)_2]\cdot 2THF$ (*anti*-**1**·2THF), *anti*-$[Mn_3(O_2CCH_3)_6(BIPhMe)_2]\cdot 2CH_2Cl_2$ (*anti*-**2A**·$2CH_2Cl_2$), *anti*-$[Mn_3(O_2CCH_3)_6(BIPhMe)_2]$ (*anti*-**2B**), *syn*-$[Mn_3(O_2CCH_3)_6(BIPhMe)_2]\cdot 3CH_2Cl_2$ (*syn*-**2**·$3CH_2Cl_2$), and $[Mn_3(O_2CCH_3)_6(phen)_2]$ (**3**)

| compound | *anti*-**1**·2THF | *anti*-**2A**·$2CH_2Cl_2$ | *anti*-**2B** | *syn*-**2**·$3CH_2Cl_2$ | **3** |
|---|---|---|---|---|---|
| formula | $C_{52}H_{70}Fe_3N_8O_{16}$ | $C_{46}H_{58}Cl_4Mn_3N_8O_{14}$ | $C_{44}H_{54}Mn_3N_8O_{14}$ | $C_{47}H_{60}Cl_6Mn_3N_8O_{14}$ | $C_{36}H_{34}Mn_3N_4O_{12}$ |
| formula weight, g $mol^{-1}$ | 1230.71 | 1253.64 | 1083.77 | 1338.57 | 879.50 |
| crystal system | monoclinic | monoclinic | triclinic | monoclinic | monoclinic |
| space group | $P2_1/c$ | $P2_1/c$ | $P\bar{1}$ | $P2_1/c$ | $C2/c$ |
| $a$, Å | 10.311 (1) | 10.754 (2) | 13.111 (3) | 12.672 (11) | 11.367 (2) |
| $b$, Å | 19.924 (3) | 19.466 (2) | 23.387 (4) | 21.422 (16) | 12.334 (1) |
| $c$, Å | 14.009 (1) | 13.724 (2) | 17.682 (3) | 22.279 (21) | 26.333 (3) |
| $\alpha$, deg | | | 71.86 (2) | | |
| $\beta$, deg | 102.563 (6) | 100.735 (7) | 111.32 (2) | 100.36 (5) | 99.11 (1) |
| $\gamma$, deg | | | 97.25 (2) | | |
| $V$, $Å^3$ | 2809 (1) | 2823 (1) | 4799 (4) | 5949 (9) | 3645.2 (9) |
| $Z$ | 2 | 2 | 4 | 4 | 4 |
| $T$, °C | −75 | −75 | −75 | −75 | −75 |
| $\rho_{calcd}$, g $cm^{-3}$ | 1.455 | 1.389 | 1.500 | 1.494 | 1.602 |
| crystal dimensions, mm | 0.45 × 0.20 × 0.20 | 0.11 × 0.12 × 0.15 | 0.12 × 0.22 × 0.22 | 0.30 × 0.40 × 0.23 | 0.25 × 0.20 × 0.13 |
| transmission factor range | 0.944–1.000 | 0.902–1.000 | 0.804–1.000 | 0.878–1.000 | 0.699–1.000 |
| linear absrptn coeff, $cm^{-1}$ | 8.4 | 8.9 | 8.2 | 9.4 | 10.5 |
| data collected | $3° \le 2\theta \le 45°$, $+h,+k,\pm l$ | $3° \le 2\theta \le 48°$, $\pm h,+k,+l$ | $3° \le 2\theta \le 45°$, $+h,\pm k,\pm l$ | $3° \le 2\theta \le 45°$, $\pm h,+k,+l$ | $3° \le 2\theta \le 25°$, $\pm h,\pm k,\pm l$; $25° \le 2\theta \le 50°$, $+h,+k,\pm l$ |
| total no. of data collected | 4099 | 4788 | 13419 | 8532 | 5097 |
| $R_{av}$ for reflcn averaging | 0.025 | 0.076 | 0.019 | 0.042 | 0.035 |
| no. of independent data | 3791 | 4582 | 12416 | 8017 | 3494 |
| no. of unique data with $I > 3\sigma(I)$ | 2590 | 2501 | 8447 | 4771 | 1845 |
| no. of variables | 358 | 358 | 803 | 703 | 249 |
| $R^b$ | 0.043 | 0.064 | 0.057 | 0.058 | 0.065 |
| $R_w{}^c$ | 0.056 | 0.076 | 0.075 | 0.080 | 0.083 |
| $p^c$ | 0.05 | 0.05 | 0.05 | 0.05 | 0.05 |

[a] Data collected on an Enraf-Nonius CAD4-F $\kappa$ geometry diffractometer with graphite monochromatized Mo K$\bar{\alpha}$ radiation ($\bar{\lambda}$ = 0.71073 Å). [b] $R = \sum||F_o| - |F_c||/\sum|F_o|$. [c] $R_w = [\sum w(|F_o| - |F_c|)^2/\sum w|F_o|^2]^{1/2}$, where $w = 4F^2/\sigma^2(F^2)$ and $\sigma^2(F^2) = [S^2(C + 4B) + (pI)^2]/(Lp)^2$ with $S$ = scan rate, $C$ = peak counts, $B$ = sum of left and right background counts, $I$ = reflection intensity, $Lp$ = Lorentz–polarization factor, and $p$ is a constant employed to avoid overweighting of intense reflections.

resulting clear, pale yellow solution stand open to the air.

**Magnetic Susceptibility Studies of 1 and 2.** Solid state magnetic susceptibility measurements on 33.3 mg of **1** and 33.4 mg of **2** were made at 3 and 10 kG, respectively, by using an SHE Model 905 SQUID-type magnetometer. A total of 47 data points was collected over a temperature range of 4.41–300 K for **1**, while 66 data points were collected over the temperature range 2.04–300 K for **2**. The susceptibilities of **1** and **2** were determined to be field-independent at the applied fields used during the temperature-dependent studies, but a significant field-dependence of the susceptibilities was noted above 5 kG for **1** and 10 kG for **2**. The susceptibilities of the Si-Al (**2**) and Kel-F polymer (**1**) sample holders were measured at the same fields and temperatures as the samples to allow for accurate correction for their contribution to the total measured susceptibilities. Diamagnetic corrections of $-556.8 \times 10^{-6}$ and $-559.8 \times 10^{-6}$ emu $G^{-1}$ $mol^{-1}$ were calculated for **1** and **2**, respectively, by using Pascal's constants.[32,33]

**Mössbauer Spectroscopy.** A standard, constant velocity spectrometer was employed to record the Mössbauer spectrum of **1** at zero applied field and 4.2 K. Values are referenced to iron metal at room temperature.

**X-ray Crystallography.** Intensity data for *anti*-**1**·2THF, *anti*-**2A**·$2CH_2Cl_2$, *anti*-**2B**, *syn*-**2**·$3CH_2Cl_2$, and **3** were collected on an Enraf-Nonius CAD4-F diffractometer equipped with an Enraf-Nonius FR558NH liquid nitrogen cryostat. Graphite monochromatized Mo K$\bar{\alpha}$ radiation ($\bar{\lambda}$ = 0.71073 Å) was employed for all studies. Crystals were mounted on the tips of glass fibers with silicone grease. In the case of **1**, care was taken to bathe the colorless crystal in nitrogen gas during all manipulations. Colorless crystals of **2** and yellow crystals of **3**, being less air-sensitive than crystals of **1**, were simply manipulated quickly in air and then placed in the nitrogen gas cold stream of the cryostat for data collection. Crystals of *anti*-**1**·2THF, *anti*-**2A**·$2CH_2Cl_2$, and *syn*-**2**·$3CH_2Cl_2$ were all determined to have $2/m$ Laue symmetry by study on the diffractometer, and space group $P2_1/c$ ($C_{2h}^5$, no. 14)[34] was chosen for all three crystals based on the systematic absences $0k0$, $k \neq 2n$; $00l$, $l \neq 2n$. Study of a crystal of **3** on the diffractometer revealed that it also had $2/m$ Laue symmetry, but space group $C2/c$ ($C_{2h}^6$, no. 15)[34] was chosen as a result of the additional centering condition, $hkl$, $h+k = 2n$. The crystal of *anti*-**2B** was determined to have $\bar{1}$ Laue symmetry, and space group $P\bar{1}$ ($C_i^1$, no. 2)[34] was chosen. Searches for higher symmetry were carried out with the program TRACER[35] in all cases, and none was found. The choices of space groups for the five crystals were confirmed by the successful solution and refinement of the structures. No loss in intensity was observed for monitored reflections in the cases of *anti*-**1**·2THF, *anti*-**2A**·$2CH_2Cl_2$, and *anti*-**2B**, thus deeming a decay correction unnecessary. A small decrease in the intensities of the monitored reflections was observed for *syn*-**2**·$3CH_2Cl_2$ (4.2%) and **3** (2.3%) and a correction for decay was applied to all data for these crystals. Data were corrected for Lorentz and polarization effects. Azimuthal $\psi$ scans were measured for several reflections from each of the crystals. The range of transmission coefficients determined from a preliminary calculation based on the $\psi$ scans[36] was small in the case of *anti*-**1**·2THF and no correction was applied for absorption. An empirical absorption correction[36] was applied to all data for *anti*-**2A**·$2CH_2Cl_2$, *anti*-**2B**, *syn*-**2**·$3CH_2Cl_2$, and **3** based on the measured $\psi$ scan data. Crystal data and details of data collection and reduction for all five compounds are given in Table I; general procedures for structural studies in our laboratory are described elsewhere.[37,38]

The structures of the compounds were solved by using either the direct methods program MITHRIL[39] or SHELX-86,[40] sometimes in combination with DIRDIF.[41] Structure refinement was carried out with the full matrix least-squares program of TEXSAN.[42] Neutral atom scattering factors were obtained from ref 43. The function minimized during refinement was $\sum w(|F_o| - |F_c|)^2$ (see Table I for the definition of $w$). Anisotropic thermal parameters were refined for all non-hydrogen atoms, except in

(32) O'Connor, C. J. *Prog. Inorg. Chem.* **1982**, *29*, 203.
(33) Mabbs, F. E.; Machin, D. J. *Magnetism and Transition Metal Complexes*; Chapman and Hall: London, 1973.
(34) *International Tables for Crystallography Volume A*; Hahn, T., Ed.; Kluwer Academic: Dordrecht, 1989; pp 174, 182, 104.
(35) Lawton, S. L. TRACER II, *A Fortran Lattice Transformation-Cell Reduction Program*; Mobil Oil Corporation: Paulsboro, NJ, 1967.
(36) North, A. C. T.; Phillips, D. C.; Mathews, F. S. *Acta Crystallogr.* **1968**, *A24*, 351.
(37) Carnahan, E. M.; Rardin, R. L.; Bott, S. G.; Lippard, S. J., to be submitted for publication.
(38) Silverman, L. D.; Dewan, J. C.; Giandomenico, C. M.; Lippard, S. J. *Inorg. Chem.* **1980**, *19*, 3379.
(39) Gilmore, G. J. *J. Appl. Cryst.* **1984**, *17*, 42.
(40) Sheldrick, G. M. In *Crystallographic Computing 3*; Sheldrick, G. M., Krüger, C., Goddard, R., Eds.; Oxford University Press: Oxford, 1985; p 175.
(41) Pathasarathi, V.; Beurskens, P. T.; Slot, J. J. B. *Acta Crystallogr.* **1983**, *A39*, 860.
(42) TEXSAN: *Single Crystal Structure Analysis Software, Version 5.0*; Molecular Structure Corporation: The Woodlands, TX, 1989.
(43) Stewart, R. F.; Davidson, E. R.; Simpson, W. T. *J. Chem. Phys.* **1965**, *42*, 3175.

the case of *anti*-**2B**, where all carbon atoms were refined isotropically in order to reduce the number of least-squares parameters. Hydrogen atom coordinates were calculated so as to place them in idealized positions, with $d$(C–H) = 0.95 Å, and their thermal parameters were fixed at 1.2 × $B_{eq}$, where $B_{eq}$ is the equivalent isotropic thermal parameter of the atom to which the hydrogen atom is attached. Computations were carried out on either a DEC VAXstation II or a DEC VAXstation 3100.

Some disorder in one of the THF solvent molecules was encountered during the refinement of the *anti*-**1**·2THF structure but was not modelled. As a result, the equivalent isotropic thermal parameters for these atoms are large. For *anti*-**2A**·$2CH_2Cl_2$, a 2-fold axial disorder was encountered in the $CH_2Cl_2$ solvent molecule. Occupancies were fixed at 0.50 for Cl1S and Cl1s and at 0.60 for Cl2S and 0.40 for Cl2s to model this disorder. At convergence, the largest ratio of parameter shift to estimated standard deviation was <0.01 for all structures. For *anti*-**1**·2THF, the largest remaining unassigned peak on the final difference Fourier map was 0.37 e Å$^{-3}$, located near the disordered THF solvent molecule; for *anti*-**2A**·$2CH_2Cl_2$, the largest residual peak on the final difference Fourier map was 0.99 e Å$^{-3}$, located near one of the $CH_2Cl_2$ solvent molecule chlorine atoms; for *anti*-**2B**, the largest unassigned peak on the final difference Fourier map was 0.71 e Å$^{-3}$, located near one of the methylimidazole methyl groups; for *syn*-**2**·$3CH_2Cl_2$, a final difference Fourier map revealed a maximum residual peak of 0.39 e Å$^{-3}$, located near one of the BIPhMe phenyl rings; and for **3**, the largest unassigned peak on the final difference Fourier map was 1.33 e Å$^{-3}$, located near the monodentate carboxylate. Full listings of atomic parameters, thermal parameters for all atoms, bond lengths and angles, and listings of observed and calculated structure factor amplitudes for all five compounds are supplied as supplementary material (Tables S1–S20).

## Results and Discussion

**Synthesis.** The initial goal of this work was to synthesize low-valent diiron and dimanganese complexes of the bidentate, imidazole-based BIPhMe ligand by using $M(O_2CR)_2{\cdot}xH_2O$ starting materials. The first structurally characterized complex of this kind, isolated from the reaction of ferrous formate and BIPhMe, was the dinuclear complex $[Fe_2(O_2CCH)_4(BIPhMe)_2]$, **4**.[22,23] This species not only afforded a potentially open or labile coordination site where, for instance, oxygen might bind, but also displayed asymmetry similar to that observed for deoxyHr (see Scheme I), in which one iron atom is five-coordinate and the other, six-coordinate. As revealed by the present work, however, attempts to synthesize iron and manganese analogs of **4** starting from the metal acetates yielded instead the trinuclear complexes **1** and **2**.[27] The linear structure adopted by these species is unprecedented in iron chemistry, although a related complex has just been communicated,[44] and has been reported only recently for manganese (vide infra).[10,45] We can only speculate why the replacement of formate by acetate ligands leads to this new structure. Since the difference in p$K_a$ values between acetic (p$K_a$ = 4.75) and formic acids (p$K_a$ = 3.75) has not hindered the synthesis of diferric model complexes of similar structure with both of these carboxylates,[17] the difference is probably steric and not electronic in nature. In particular, the methyl group of the monodentate bridging acetate in a dinuclear structure such as **4** might block the coordination of BIPhMe to the iron toward which the methyl group is directed, leading to the formation of **1** or **2**.

The reaction used to prepare the trinuclear complexes **1** and **2** (eq 1) is not restricted to BIPhMe. Other bidentate, nitrogen-donating ligands may be employed, as evidenced by the synthesis of $[Mn_3(O_2CCH_3)_6(phen)_2]$, **3**, $[Mn_3(O_2CPh)_6(bpy)_2]$, **5**,[10,24] and $[Mn_3(O_2CCH_3)_6(bpy)_2]$, **6**,[45] by similar methods. The preparation of complexes containing dimetallic tricarboxylate-bridged units such as those observed in **1**–**4** and **5** and **6** may depend on the metal precursor employed in the reaction. Thus far, such complexes have been synthesized only from $M(O_2CR)_2{\cdot}xH_2O$ starting materials.

$$3M(O_2CR)_2{\cdot}xH_2O + 2L \rightarrow [M_3(O_2CR)_6L_2] \qquad (1)$$

**Description of the Structures.** Complexes **1**–**3** consist of a linear array of divalent metals (Figures 1–5). The central metal, which

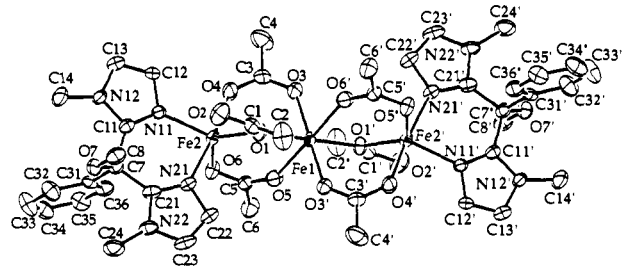

Figure 1. ORTEP[87] drawing showing 40% probability ellipsoids and labeling scheme for *anti*-$[Fe_3(O_2CCH_3)_6(BIPhMe)_2]{\cdot}2THF$, *anti*-**1**. The solvent molecules and hydrogen atoms are omitted for clarity.

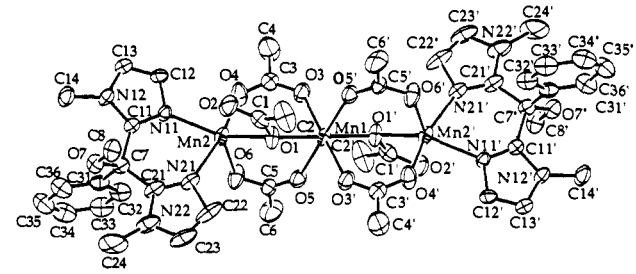

Figure 2. ORTEP[87] drawing showing 40% probability ellipsoids and labeling scheme for *anti*-$[Mn_3(O_2CCH_3)_6(BIPhMe)_2]{\cdot}2CH_2Cl_2$, *anti*-**2A**. The solvent molecules and hydrogen atoms are omitted for clarity.

is located on a crystallographic inversion center in *anti*-**1**·2THF and *anti*-**2A**·$2CH_2Cl_2$ and on a $C_2$ axis in **3**, is coordinated octahedrally by six acetate oxygen atoms. Four acetate groups form bridges to the two flanking metals in the familiar bidentate fashion, whereas the other two use the less common monodentate mode. These latter, monodentate acetates coordinate one oxygen atom as a monoatomic bridge between the metals, while the second oxygen atom is free to interact with another metal or to "dangle" freely in space. Such units are known but uncommon in metal carboxylate chemistry.[46-59] The termini of the $\{M(O_2CCH_3)_3M(O_2CCH_3)_3M\}$ units are capped by BIPhMe or phen ligands, resulting in five-coordination at these sites.

The dangling oxygen atoms of the monodentate acetates interact weakly with the terminal metal in some cases and block the potential sixth coordination site of the terminal metals in all cases. Several factors reveal the existence of a weak interaction between the dangling oxygen atoms ($O_d$, see Figure 6) and the terminal metals ($M_{int}$) in **1**–**3**. Firstly, the monodentate acetates are oriented such that $O_d$ points toward $M_{int}$ in all of the structurally characterized forms of **1**–**3**. Secondly, the $M_{int}\cdots O_d$ contacts are relatively short in some of the structures, indicating at least a weak interaction. Thirdly, the C–O bonds in the monodentate car-

(44) Vankai, V. A.; Newton, M. G.; Kurtz, D. M., Jr. *Inorg. Chem.* **1992**, *31*, 341.
(45) Ménage, S.; Vitols, S. E.; Bergerat, P.; Codjovi, E.; Kahn, O.; Girerd, J.-J.; Guillot, M.; Solans, X.; Calvet, T. *Inorg. Chem.* **1991**, *30*, 2666.
(46) Mehrotra, R. C.; Bohra, R. *Metal Carboxylates*; Academic: New York, 1983.
(47) Alcalá, R.; Fernandéz Garciá, J. *Rev. Acad. Cienc. Exactas Fis. Quim. Nat. Zaragoza* **1973**, *28*, 305.
(48) Cotton, F. A.; Diebold, M. P.; Matusz, M.; Roth, W. J. *Inorg. Chim. Acta* **1986**, *112*, 147.
(49) Mak, T. C. W.; Yip, W.-H.; O'Reilly, E. J.; Smith, G.; Kennard, C. H. *Inorg. Chim. Acta* **1985**, *100*, 267.
(50) Lis, T. *Acta Crystallogr.* **1977**, *B3*, 2694.
(51) Post, M. L.; Trotter, J. *J. Chem. Soc., Dalton Trans.* **1974**, 674.
(52) Clegg, W.; Little, I. R.; Straughan, B. P. *Acta Crystallogr.* **1986**, *C42*, 1319.
(53) Puff, H.; Sievers, R.; Elsner, G. *Z. Anorg. Allg. Chem.* **1975**, *413*, 37.
(54) Freeman, H. C.; Huq, F.; Stevens, G. N. *J. Chem. Soc., Chem. Commun.* **1976**, 90.
(55) Prout, K.; Carruthers, J. R.; Rossotti, F. J. C. *J. Chem. Soc. A* **1971**, 3350.
(56) Catterick, J.; Thornton, P. *J. Chem. Soc., Dalton Trans.* **1976**, 1634.
(57) Clegg, W.; Little, I. R.; Straughan, B. P. *J. Chem. Soc., Dalton Trans.* **1986**, 1283.
(58) Clegg, W.; Little, I. R.; Straughan, B. P. *J. Chem. Soc., Chem. Commun.* **1985**, 73.
(59) Clegg, W.; Little, I. R.; Straughan, B. P. *Inorg. Chem.* **1988**, *27*, 1916.

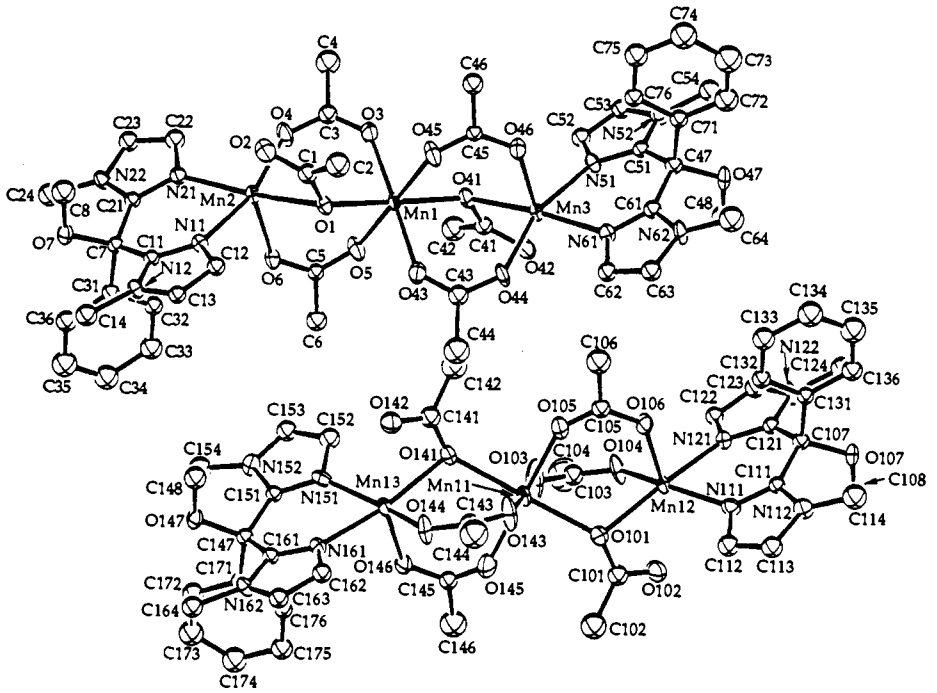

**Figure 3.** ORTEP[87] drawing showing 40% probability ellipsoids and labeling scheme for the two independent molecules of **2** in the *anti*-$[Mn_3(O_2CCH_3)_6(BIPhMe)_2]$, *anti*-**2B**, structure. Hydrogen atoms are omitted for clarity.

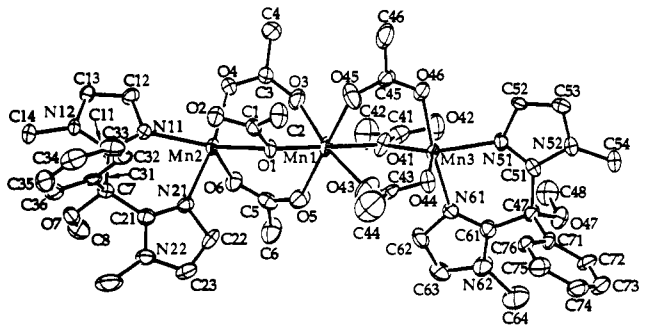

**Figure 4.** ORTEP[87] drawing showing 40% probability ellipsoids and labeling scheme for *syn*-$[Mn_3(O_2CCH_3)_6(BIPhMe)_2]\cdot 3CH_2Cl_2$, *syn*-**2**. The solvent molecules and hydrogen atoms are omitted for clarity.

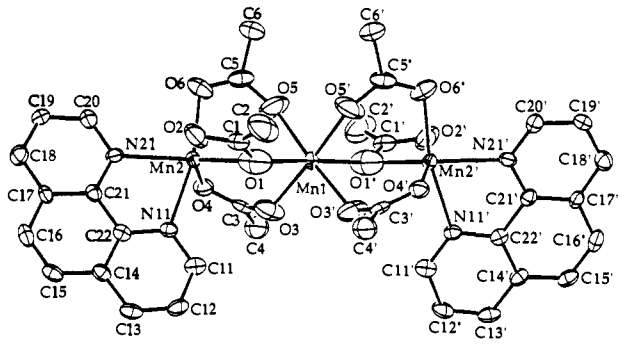

**Figure 5.** ORTEP[87] drawing showing 40% probability ellipsoids and labeling schemes for $[Mn_3(O_2CCH_3)_6(phen)_2]$, **3**. Hydrogen atoms are omitted for clarity.

boxylates are relatively symmetric in some of the structures, indicating delocalization of the double bond over the O–C–O unit, consistent with an interaction occurring between $M_{int}$ and $O_d$. Fourthly, the trigonal-bipyramidal coordination geometry of the terminal metals is distorted toward octahedral geometry in some cases. A good measure of this distortion is the $N_p$–$M_{int}$–O angle (see Figure 6) in the trigonal plane which is bisected by the $M_{int}\cdots O_d$ vector. In the case of *anti*-**1**, N(11)–Mn(2)–O(1) is 124.6 (1)°, very close to the idealized trigonal-bipyramidal value of 120°. This complex also has the longest $M_{int}\cdots O_d$ contact, 3.005 (4) Å.

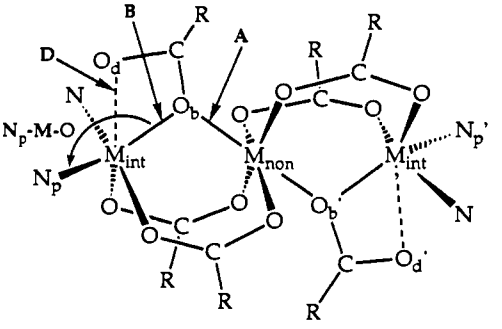

**Figure 6.** The general structure of **1–3**, showing the dangling ($O_d$) and the bridging ($O_b$) oxygen atoms of the monodentate carboxylates, the central metal, $M_{non}$, which does not interact with $O_d$, and the terminal metals, $M_{int}$, which interact with $O_d$. The $M_{int}\cdots O_d$, $M_{int}\cdots O_b$ and $M_{non}\cdots O_b$ contacts as well as the angle bisected by $O_d$ in the trigonal plane of the $M_{int}$ coordination sphere are shown.

**Chart II**

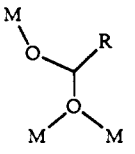

The shortest $M_{int}\cdots O_d$ contact, 2.306 (5) Å, occurs in *anti*-**2B**, and the $N_p$–$M_{int}$–O angle, N(11)–Mn(2)–O(4), is 163.7 (2)° in this case, much closer to the octahedral value of 180°. Further comparisons of pertinent metrical parameters for the structures of **1–4** as well as **5** and **6** are made in Table II. A more detailed analysis of the structural trends that arise in complexes containing monodentate bridging carboxylates may be found elsewhere.[28]

The linear structures of **1–3** are a striking departure from that of the triangular oxo-centered "basic" metal carboxylates, $\{M_3O(O_2CR)_6L_3\}$,[10,26] and the variants thereof[60] that have been the dominant structural motif in triiron and trimanganese chemistry for many years. That is not to say, however, that such linear trinuclear structures are without precedent. In fact, an examination of the crystal structure of polymeric $Mn(O_2CCH_3)_2\cdot 4H_2O$[61]

(60) Gorun, S. M.; Lippard, S. J. *J. Am. Chem. Soc.* **1985**, *107*, 4568.

**Table II.** Pertinent Structural Parameters[a] for **1–3**, **4**,[22,23] and **5** and **6**[45,86]

| complex | *B* (Å) | *D* (Å) | *A* (Å) | M–M (Å) | C–$O_b$ (Å) | C–$O_d$ (Å) | $N_p$–M–$O_b$ (deg) |
|---|---|---|---|---|---|---|---|
| *anti*-$[Fe_3(O_2CCH_3)_6(BIPhMe)_2]\cdot 2THF$ (**1**·2THF) | 2.027 (3) | 3.005 (4) | 2.151 (3) | 3.3251 (9) | 1.305 (6) | 1.232 (6) | 124.6 (1) |
| $[Fe_2(O_2CH)_4(BIPhMe)_2]$ (**4**) | 2.113 (2) | 2.787 (3) | 2.172 (2) | 3.5736 (8) | 1.270 (4) | 1.214 (4) | 146.7 (1) |
| *anti*-$[Mn_3(O_2CCH_3)_6(BIPhMe)_2]\cdot 2CH_2Cl_2$ (*anti*-**2A**·$2CH_2Cl_2$) | 2.172 (5) | 2.488 (7) | 2.205 (5) | 3.635 (1) | 1.28 (1) | 1.22 (1) | 142.5 (2) |
| *anti*-$[Mn_3(O_2CCH_3)_6(BIPhMe)_2]$ (*anti*-**2B**) | 2.269 (4) | 2.306 (5) | 2.234 (4) | 3.700 (2) | 1.269 (8) | 1.254 (8) | 163.6 (2) |
| | 2.258 (4) | 2.344 (5) | 2.238 (9) | 3.716 (2) | 1.275 (7) | 1.246 (8) | 160.9 (2) |
| | 2.264 (5) | 2.319 (5) | 2.240 (5) | 3.658 (2) | 1.287 (8) | 1.239 (8) | 158.3 (2) |
| | 2.238 (5) | 2.314 (5) | 2.248 (5) | 3.691 (2) | 1.274 (8) | 1.252 (8) | 161.0 (2) |
| *syn*-$[Mn_3(O_2CCH_3)_6(BIPhMe)_2]\cdot 3CH_2Cl_2$ (*syn*-**2**·$3CH_2Cl_2$) | 2.242 (6) | 2.370 (6) | 2.181 (6) | 3.560 (3) | 1.27 (1) | 1.25 (1) | 149.3 (2) |
| | 2.138 (6) | 2.790 (7) | 2.200 (6) | 3.370 (3) | 1.27 (1) | 1.24 (1) | 133.8 (3) |
| $[Mn_3(O_2CCH_3)_6(phen)_2]$ (**3**) | 2.285 (9) | 2.425 (6) | 2.133 (6) | 3.387 (1) | 1.263 (9) | 1.224 (9) | 137.8 (2) |
| $[Mn_3(O_2CPh)_6(bpy)_2]$ (**5**) | 2.285 (4) | 2.274 (4) | 2.239 (3) | 3.588 (1) | 1.284 (6) | 1.257 (8) | |
| $[Mn_3(O_2CCH_3)_6(bpy)_2]$ (**6**) | 2.155 (3) | 2.606 (6) | 2.201 (4) | 3.614 (1) | 1.275 (9) | 1.228 (8) | |

[a] Refer to Figure 6 for the definition of the structural parameters given in this table.

Chart III

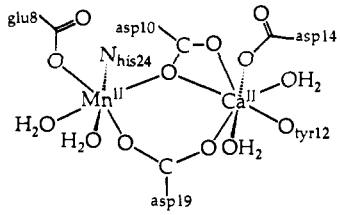


Metal center of ConA

reveals that the $\{M_3(O_2CCH_3)_6\}$ unit of **2** and **3** exists in the starting material employed to synthesize these complexes. In the polymer, however, all of the Mn(II) ions are hexacoordinate, and, rather than interacting with the terminal metals in the $\{M_3(O_2CCH_3)_6\}$ unit, the monodentate acetate dangling oxygen atoms bridge to other $\{M_3(O_2CCH_3)_6\}$ units. This bridging of the carboxylate functionality among three metal centers (Chart II) often occurs in metal carboxylate polymers (see refs 47 and 61, for example). Unlike the structure of $Mn(O_2CCH_3)_2\cdot 4H_2O$, that of the $Fe(O_2CCH_3)_2$ starting material for **1** does not contain the linear trinuclear unit, although monodentate bridging carboxylates are present.[47] As noted previously, the $\{(BIPhMe)M(O_2CCH_3)_3M\}^+$ unit comprising half of complexes **1** and **2** is structurally analogous to **4**. The structures of **1–3** are also similar to those of **5**[10] and **6**[45] as well as to a series of homo- and heterotrinuclear complexes, $[M_2M'(O_2CR)_6B_2]$ (M = M' = Co, Zn; M = Zn, M' = Mg, Ca, Sr, Co, Ni, Mn, Cd; B is a monodentate base), that have been studied extensively.[56–59,62,63] Finally, several linear trinuclear complexes, $[Mn_3(O_2CCH_3)_4(saladhp)_2(CH_3OH)_2]$[24,64] and $[M_3(O_2CCH_3)_2(salpn)_2(DMF)]$ (M = Co, Fe),[24,65] which bear some resemblance to complexes **1–3**, have been reported.

The occurrence of the $\{M(O_2CR)_3M\}^+$ moiety in complexes **1–6** and the homo- and heterotrinuclear complexes of the form $[M_2M'(O_2CR)_6B_2]$ as well as in the structure of polymeric $Mn(O_2CCH_3)_2\cdot 4H_2O$, gives precedence to the possibility that this type of tricarboxylate-bridged dimetal unit may play a role in the structure and function of metalloproteins. At present, a monodentate carboxylate is known to exist only in concanavalin A, ConA (Chart III).[66] Similar metal center structures have been postulated to occur in some related proteins.[67,68] It is interesting to note that ConA was initially proposed to contain two bidentate bridging carboxylates based on a lower resolution structure of the protein.[69]

The availability of several crystalline forms of **2** has allowed us to examine aspects of structural variability in this complex. The difference between the syn and anti isomers of **2** is one feature of interest. Isomerization from *syn*-**2** to *anti*-**2** interchanges the positions in the coordination sphere of one of the imidazole nitrogen atoms and the dangling oxygen atom, $O_d$, leading to a configuration where the BIPhMe ligands lie on opposite sides of the plane defined by the $O_d$ and metal atoms (Chart IV). Thus, if the positions of O42 and N61 are swapped in *syn*-**2** (Figure 4), the anti isomer is obtained. In the anti isomer, the local $C_3$ axes of the terminal metal atoms are antiparallel, as required by the crystallographic inversion center in the molecule. In the syn isomer, the local $C_3$ axes subtend an angle of 47° with respect to one another. In both *syn*- and *anti*-**2A**, the monodentate bridging oxygen atoms are located in the trigonal planes of the terminal metals. This is not the case in *anti*-**2B**, where the $O_b$ atoms are located on the local $C_3$ axes. Other than this difference, the two molecules in the *anti*-**2B** structure are relatively similar to *anti*-**2A**.

An interesting feature of the *syn*-**2** structure is the presence of one bidentate carboxylate ligand that is actually poised between monodentate and bidentate bridging modes (Figure 4). Its geometry is characterized by a short Mn(3)···O(43) contact of 2.601 (8) Å compared to similar distances for the other bidentate bridging carboxylates in the molecule, which range from 3.286 (7) to 3.382 (7) Å in *syn*-**2**. A lengthening of the Mn(3)–O(44) bond to 2.228 (7) Å, compared to the distances of 2.120 (6)–2.141 (6) Å observed for similar bonds in the *syn*-**2** structure, also demonstrates this rocking of the carboxylate comprising C(43), C(44), O(43), and O(44) toward the monodentate bridging mode. It is interesting to note by comparison that, in $Fe(O_2CCH_3)_2$, a unit occurs having two monodentate bridging carboxylates and one bidentate bridging carboxylate.[47] This type of bridging is also seen in $[Cu_2(O_2CCH_3)_3(BIPhMe)_2](BF_4)$,[70] and cases where two monodentate carboxylates bridge two Cu(II) centers are fairly common.[28]

The metrical parameters for *anti*-**2A**·$2CH_2Cl_2$, *anti*-**2B**, and *syn*-**2**·$3CH_2Cl_2$ reveal that the tricarboxylate-bridged unit can accommodate a considerable degree of flexibility. For instance, the Mn···Mn distances range from 3.370 (3) to 3.715 (2) Å. These values fall within the range observed for di- and tribridged dimanganese(II) complexes,[8,71] but a variation of 0.345 Å in the metal–metal distances within a single structural unit is extraordinary. This finding should be kept in mind when interpreting protein EXAFS data, a process that often involves the assignment of structure based on M···M distances.[72–74] Metal centers having

(61) Bertaut, E. F.; Tran Qui, D.; Burlet, P.; Thomas, M.; Moreau, J. M. *Acta Crystallogr.* **1974**, *B30*, 2234.
(62) Catterick, J.; Hursthouse, M. B.; New, D. B.; Thornton, P. *J. Chem. Soc., Chem. Commun.* **1974**, 843.
(63) Clegg, W.; Hunt, P. A.; Straughan, B. P.; Mendiola, M. A. *J. Chem. Soc., Dalton Trans.* **1989**, 1127.
(64) Li, X.; Kessissoglou, D. P.; Kirk, M. L.; Bender, C. J.; Pecoraro, V. L. *Inorg. Chem.* **1988**, *27*, 1.
(65) Gerli, A.; Hagen, K. S.; Marzilli, L. G. *Inorg. Chem.* **1991**, *30*, 4673.
(66) Hardman, K. D.; Agarwal, R. C.; Freiser, M. J. *J. Mol. Biol.* **1982**, *157*, 69.
(67) Riskulov, R. R.; Dobrokhotova, Z. D.; Kuzev, S. V.; Losanov, Y. D.; Lubnin, M. Y.; Mokulskaya, T. D.; Myshko, G. E.; Proskudina, L. T.; Rogacheva, M. M.; Saprykina, L. F.; Khrenvov, A. A.; Mokulskii, M. A. *FEBS Lett.* **1984**, *165*, 97.
(68) Bhattacharyya, L.; Brewer, C. F. *Biochemistry* **1985**, *24*, 4974.
(69) Hardman, K. D.; Ainsworth, C. F. *Biochemistry* **1972**, *11*, 4910.
(70) Rardin, R. L.; Tolman, W. B.; Cohen, S. J.; Liu, S.; Lippard, S. J., manuscript in preparation.
(71) Caneschi, A.; Ferraro, F.; Gatteschi, D.; Melandri, M. C.; Rey, P.; Sessoli, R. *Angew. Chem., Int. Ed. Engl.* **1989**, *28*, 1365.
(72) George, G. N.; Prince, R. C.; Cramer, S. P. *Science* **1989**, *243*, 789.

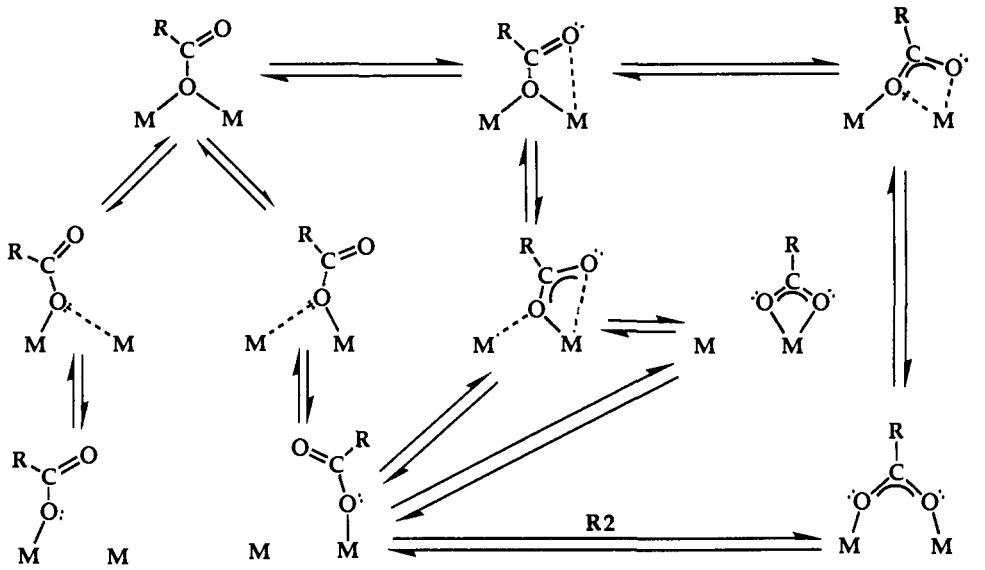


**Figure 7.** Relationships among the structures involved in the carboxylate shift.[28] The arrows labeled R2 identify the shift found for the ribonucleotide reductase R2 protein (see text).

**Chart IV**

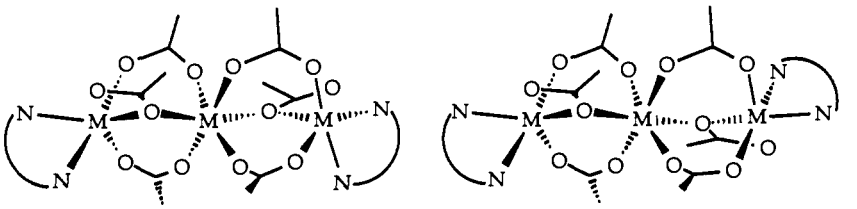

*syn*-**2** *anti*-**2**

**Chart V**

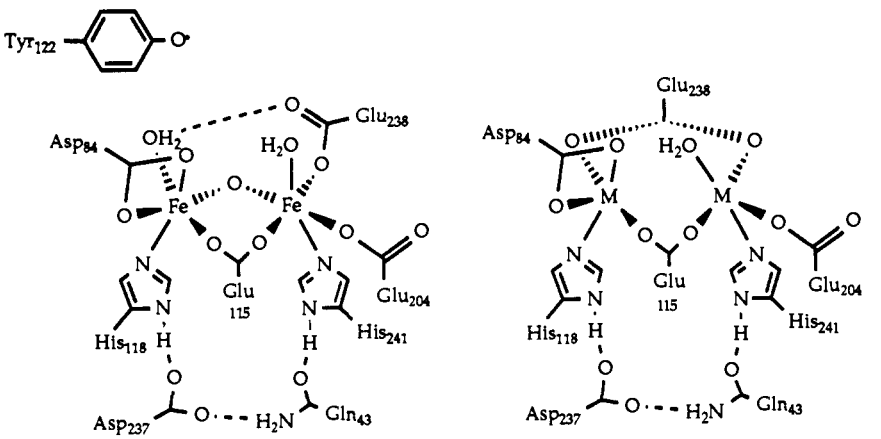


Diiron(III) Center of R2

Diiron(II) Center (M = Fe) or Dimanganese(II) (M = Mn) Derivative of R2

a tricarboxylate-bridged unit or a monodentate bridging carboxylate might result in a range of such distances.

The oxygen atoms of monodentate carboxylates interact with the bridged metals in an intriguing way in **2** as well as in **1** and **3**–**6**. As previously described,[28] there is a linear correlation between $M_{int}\cdots O_d$, D, and $M_{int}\cdots O_b$, B (Figure 6). Thus, as D decreases, B lengthens, leading ultimately to a shift of the monodentate bridging carboxylate ligand to a bidentate bridging mode. We previously referred to this process as the "carboxylate shift" and expanded the idea to include shifts to other carboxylate binding modes, including terminal (Figure 7). This concept and its biological implications are discussed in more detail in ref 28. Subsequent to our analysis, the structures of the dimanganese(II) and diiron(II) derivatives of ribonucleotide reductase protein R2 were elucidated by X-ray diffraction.[29-31] As indicated in Chart V, the carboxylate group of Glu 238 has shifted from monodentate terminal to bidentate bridging in the Mn(II) analogue, apparently displacing the water molecule on the other metal atom. No third bridging oxo, hydroxo, or aqua ligand has yet been identified in this structure. It is interesting that a similar carboxylate shift seems to occur in reduced R2,[29-31] the functionally important form

(73) Yachandra, V. K.; Guiles, R. D.; McDermott, A. E.; Cole, J. L.; Britt, R. D.; Dexheimer, S. L.; Sauer, K.; Klein, M. P. *Biochemistry* **1987**, *26*, 5974.
(74) Kirby, J. A.; Robertson, A. S.; Smith, J. P.; Thompson, A. C.; Cooper, S. R.; Klein, M. P. *J. Am. Chem. Soc.* **1981**, *103*, 5529.

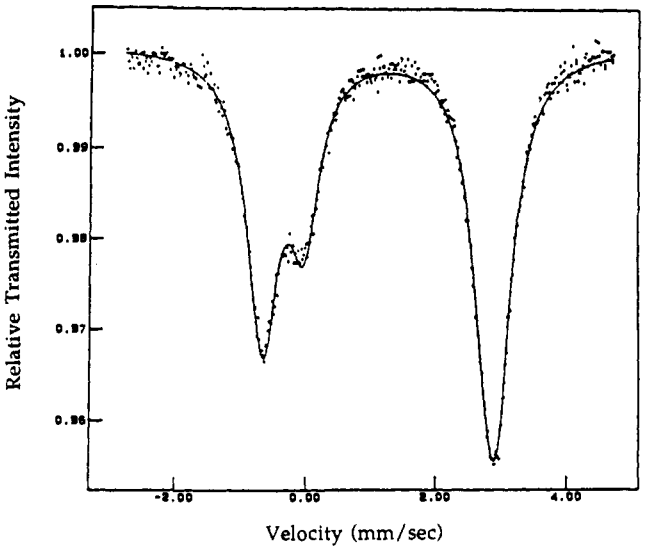


Figure 8. Zero-field Mössbauer spectrum of 1 at 4.2 K. The solid line is the best least-squares fit of the data (see text for details).

of the protein, indicating that the carboxylate shift may be an important aspect of the protein chemistry.

**Spectroscopic and Magnetic Properties.** Apart from X-ray crystallography, infrared spectroscopy might be expected to provide useful information about complexes containing carboxylates bound in various modes. Unfortunately, in the cases of **1–4**, only a single broad vibrational band occurs at ca. 1600 $cm^{-1}$, which we assign as $\nu_{asym}$ for all of the bridging carboxylates. A similar result occurs in other complexes containing both monodentate and bidentate bridging carboxylates, although bands specific to the various types of bridging carboxylates can be discerned in some cases.[59]

The Mössbauer spectrum of **1** (Figure 8) consists of two quadrupole doublets with an intensity ratio of 2:1, isomer shifts of 1.14 and 1.36 mm $s^{-1}$, respectively, and quadrupole splittings of 3.60 and 2.64 mm $s^{-1}$, respectively. Although both isomer shift values are characteristic of ferrous iron,[75] the terminal metals show a diminished shift relative to the central metal. This effect is believed to result from the presence of the $\pi$-acceptor aromatic nitrogen atoms in the coordination spheres of the terminal metal ions. The larger quadrupole splitting parameter for the terminal metals is consistent with their relatively more distorted coordination environments compared to the octahedral central metal.[75] From the Mössbauer spectra of **1** and **4**,[22,23] it appears that the quadrupole splitting for $M_{int}$ is a reasonable measure of the degree of distortion toward octahedral geometry that occurs as a result of the $M_{int}\cdots O_d$ interaction. In **1**, where the $M_{int}\cdots O_d$ interaction is very weak, judging by the D of 3.005 (4) Å and $N_p$–$M_{int}$–O angle of 124.6 (1)°, $\Delta E_Q$ is 3.60 mm $s^{-1}$. In **4**, the closer contact of 2.787 (3) Å between $M_{int}$ and $O_d$ leads to a $N_p$–$M_{int}$–O angle of 146.7 (1)°, closer to the octahedral value of 180°. The corresponding $\Delta E_Q$ for **4** is 3.30 mm $s^{-1}$, reduced significantly from that observed for **1**.

Examination of Figure 9 reveals that the effective moment ($\mu_{eff}$) of solid **1** increases from 9.19 $\mu_B$ per molecule (5.31 $\mu_B$ per metal) at 300 K to 17.29 $\mu_B$ per molecule (9.98 $\mu_B$ per metal) at 4.41 K. This rise in effective moment with decreasing temperature indicates that the complex is coupled ferromagnetically. A complex in which three $S = 2$ ions are completely ferromagnetically coupled should behave as an $S = 6$ system. In such a case, the maximum $\mu_{eff}$ should be that given by eq 2, where $S = 6$, or 12.96 $\mu_B$ per molecule if $g$ is equal to 2.0. The fact that the $\mu_{eff}$ is 17.29

$$\mu_{eff} = [g^2S(S + 1)]^{1/2} \quad (2)$$

$\mu_B$ per molecule at 4.41 K suggests that, besides intramolecular ferromagnetic coupling, there may also be some intermolecular

(75) Greenwood, N. N.; Gibb, T. C. *Mössbauer Spectroscopy*; Chapman and Hall, Ltd.: London, 1971.

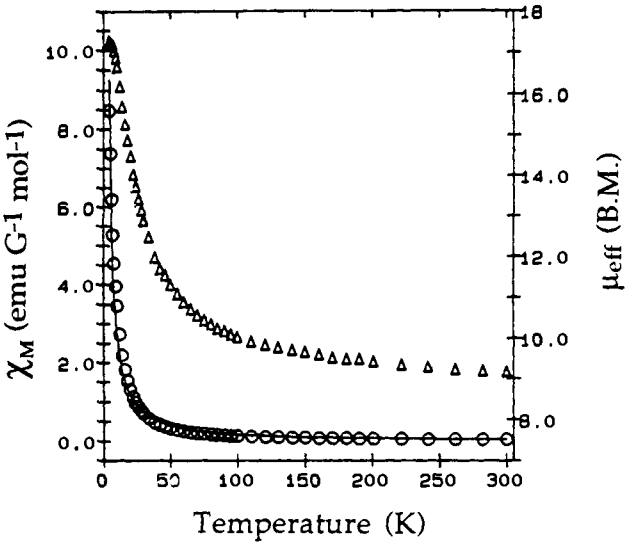


Figure 9. Plot of molar susceptibility, $\chi_M$ (O), and effective moment, $\mu_{eff}$ (Δ), for **1**. The solid line is the result of a theoretical fit to the susceptibility data with $g$ and $J_{13}$ fixed at 2.03 and 1.0, respectively, and $J$ and $\theta$ refined to +8 (6) $cm^{-1}$ and +2.07 (6) K, respectively (see text for details).

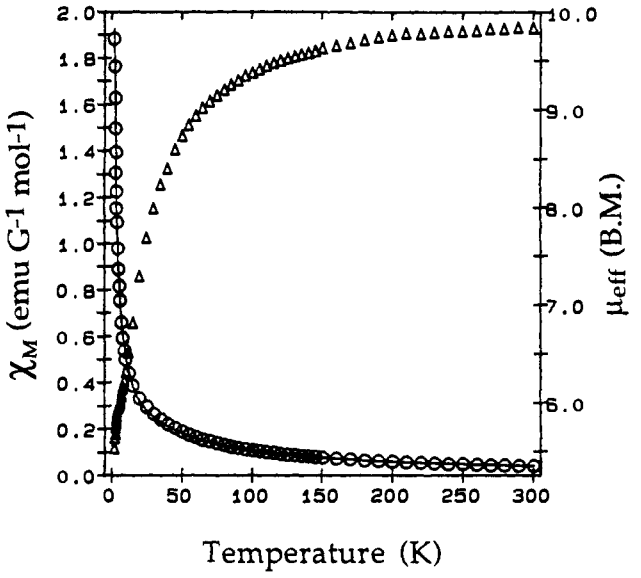


Figure 10. Plot of molar susceptibility, $\chi_M$ (O), and effective moment, $\mu_{eff}$ (Δ), for **2**. The solid line is the best theoretical fit to the data with $g$ fixed at 2.0 and $J$, $J_{13}$, and $\theta$ refined to −2.8 (1) $cm^{-1}$, −0.311 (3) $cm^{-1}$, and −0.24 (1) K, respectively (see text for details).

**Scheme II**

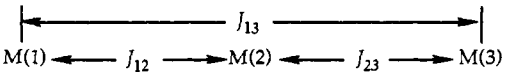


interaction which leads to a further increase in $\mu_{eff}$ at low temperature above that calculated from eq 2. The effective moment of **2** (Figure 10), in contrast to that of **1**, decreases from 9.85 $\mu_B$ per molecule (5.69 $\mu_B$ per metal) at 300 K to 5.54 $\mu_B$ per molecule (3.20 $\mu_B$ per metal) at 2.04 K. This decrease from a value approaching the spin-only moment, 5.91 $\mu_B$ per metal calculated from eq 2 for $S = 5/2$ ions, to a value of 3.20 $\mu_B$ per metal is indicative of antiferromagnetic coupling.

The interaction of the three magnetic ions in **1** and **2** (Scheme II), where the coupling constants for the intermetal interactions are as indicated, is governed by the isotropic Hamiltonian given in eq 3. Details of the derivation of the susceptibility eqs for **1**

$$\mathcal{H} = -2[J_{12}\cdot S_1\cdot S_2 + J_{13}\cdot S_1\cdot S_3 + J_{23}\cdot S_2\cdot S_3] + \mu_B[g_1S_1 + g_2S_2 + g_3S_3]\cdot H \quad (3)$$

and **2** based on eq 3 by the method described in ref 76 are given in the supplementary material (derivation S23). It should be noted that an equation for the molar susceptibility of **2** was also available from ref 77, and the results obtained from fitting this expression to the data for **2** were identical to fits to the data of the formula derived from eq 3. The derived temperature-dependent susceptibility formulae were fit to the data for **1** and **2** by using a general least-squares fitting program.[78] The best fits for **1** and **2** are shown with the observed data in Figures 9 and 10, respectively.

Variables employed to fit the data for **1** were $J$, $J_{13}$, $g$, and $\theta$. Attempts to fit the susceptibility equation to the data by allowing all variables to refine independently resulted either in divergence of the refinement or results that were not physically meaningful, for example, $g > 2.5$. After several trials, it was determined that the best results were obtained with variation of $J$ and $\theta$, $J_{13}$ fixed at 1.0 $cm^{-1}$, and $g$ fixed at 2.03. Refinement in this manner did not lead to convergence, however. Although $\theta$ refined to 2.07 (6) K, $J$ continued to oscillate between +5 and +10 $cm^{-1}$, with standard deviations of 5–6 $cm^{-1}$. From this behavior, we conclude that variation of $J$ in the range +5 to +10 $cm^{-1}$ has little effect on the overall susceptibility function, which was confirmed by calculating susceptibilities by derivation S23 with $J$ values in the range +5 to +10 $cm^{-1}$. Thus, $J$ cannot be determined more accurately by this analysis. This result could be the effect of neglecting zero field splitting, since systems where $J$ is on the order of the zero field splitting are known to have multiple solutions.[79] What can be concluded from these results is that the metals in **1** are coupled ferromagnetically with a $J$ value probably lying between +4 and +11 $cm^{-1}$. This result is interesting, especially by comparison to the $J$ values obtained for other polyiron species with bridging oxygen atoms, which are usually coupled antiferromagnetically.[80] There are several examples in the literature of ferromagnetically coupled diiron species. The diiron(II,III) complex, $[Fe_2(salamp)_2]^{1-}$,[24] was reported to exhibit an $S = 9/2$ ground state as a result of ferromagnetic coupling.[81,82] The mixed valence dinuclear complex $[Fe_2(Me_3TACN)_2(OH)_3]^{2+}$ has also been reported to exhibit an $S = 9/2$ ground state.[24,83] EPR spectroscopic studies of the diiron complex, $[Fe_2(bpmp)(O_2CR)_2]BPh_4$,[24] suggest that it, too, displays ferromagnetic coupling.[84] Additionally, azidodeoxyHr[79] and the diiron(II,II) form of the hydroxylase component of MMO[85] are believed to display ferromagnetic coupling. Complex **1** appears to be the first ferromagnetically-coupled triiron(II) species with bridging oxygen atoms.

Initial attempts to fit the observed susceptibility data for **2** were made by using the Curie–Weiss law, but a very poor fit was obtained. A fit of the derived susceptibility equation to the data with only $J$ varied and $J_{13}$ and $\theta$ set equal to zero gave an inferior, but reasonable, approximation of the observed data. The $J$ value refined to −4.8 (6) $cm^{-1}$ in this case, very similar to the result of −4.4 $cm^{-1}$ obtained for **6** when fit in a similar fashion.[45] If $J$ and $J_{13}$ were allowed to vary with $\theta$ remaining fixed at zero, a much better fit was obtained than in the previous case, but a minor discrepancy between the $\chi_{obs}$ and $\chi_{fit}$ at the lowest temperatures was evident. In this case, $J$ and $J_{13}$ refined to −1.86 (6) and −0.311 (8) $cm^{-1}$. The best fit (Figure 10) was obtained when $J$, $J_{13}$, and $\theta$ were allowed to vary simultaneously, refining to values of −2.8 (1) $cm^{-1}$, −0.09 (3) $cm^{-1}$, and −0.24 (1) K, respectively. The theoretical susceptibilities were in better agreement with the experimental data in this case than in either of the previous cases. The negative value of $\theta$ indicates that some intermolecular antiferromagnetic coupling may occur in **2**. The values of $J$ obtained from these fits indicate that only weak antiferromagnetic coupling is mediated by the monodentate bridging carboxylate in these complexes. It is not surprising that the monodentate bridging carboxylate does not mediate a large degree of coupling in **2**, due to the fact that the $Mn–O_b$ distances are relatively long (see Table II). The coupling displayed in **2** is even weaker than the coupling observed for hydroxide- and alkoxide-bridged species.[80]

**Reaction Chemistry of 1 and 2.** Complex **1** is fairly robust. Although it appeared that ligands such as halides might bind readily to the potential sixth coordination sites of the terminal metals in **1**, the only product isolated from reactions of **1** with $Et_4NBr$, $Et_4NCl$, NaF, or imidazole in methanol at room temperature or 55 °C was starting material, as determined by IR spectroscopy, elemental analysis, or X-ray crystallography. Attempts to react **1** with NO resulted in decomposition. Complex **1** is stable in water up to pH 10 and can even be recrystallized from this solvent. The dangling oxygen atom evidently provides good protection of the sixth coordination site, blocking the binding of other ligands and preventing hydrolysis of the complex. As further evidence for the stability of the linear trinuclear complex, we note that the reaction of **4** with excess acetate in methanol yields **1**, as determined by X-ray crystallography.

Both **1** and **2** react with dioxygen. Exposure of chloroform solutions of **1** to air results in a brown solution. Brown-red solutions are also obtained if solutions of **2** are left open to air, but the reaction is slow and occurs over days to weeks in the case of **2**. Complex **4** has been shown to react with dioxygen to give a ($\mu$-oxo)bis($\mu$-carboxylato)diiron(III) complex, $[Fe_2O(\mu\text{-}O_2CH)_2(O_2CH)_2(BIPhMe)_2]$, **7**.[22,23] By analogy to this reaction, we might expect $\mu$-oxo species to be the products of reactions of **1** and **2** with dioxygen, as well. Although many attempts have been made to isolate crystalline products from these reactions, only very small crystals unsuitable for X-ray diffraction studies have been obtained. Studies of this system are continuing.

The type of oxygen reactivity that **4** displays illustrates the chemistry that might occur when the diferrous form of ribonucleotide reductase reacts with dioxygen. As already mentioned, the ($\mu$-oxo)($\mu$-carboxylato)diiron(III) center of oxidized R2 also has two bound terminal carboxylates (see Chart V), similar to those observed in **7**. We suggested that one of the terminal carboxylates in oxidized RR might be bridging in reduced RR, similar to the structure of **4**.[27] Indeed, one of the monodentate carboxylates has shifted to a bridging mode in the dimanganese(II) and diiron(II) forms of the protein (Chart V).[29–31]

## Conclusions

Reaction of divalent iron and manganese carboxylates with bidentate nitrogen-donating ligands has produced some intriguing complexes. The structural trends displayed in **1–3** and **4** as well as in **5** and **6** illustrate many important features of metal carboxylate chemistry and the relationships among the various carboxylate binding modes. The structural motif of the linear trinuclear $\{M_3(O_2CR)_6\}$ (M = Fe, Mn) unit may turn out to be as important as that of the triangular basic carboxylate structure, which is characteristic of the trivalent and mixed valent $M^{II}M_2^{III}$ analogues. Also of interest are the magnetic properties of **1** and **2**. Complex **1** is a rare example of a ferromagnetically-coupled polyiron complex with bridging oxygen atoms, while **2** displays weak antiferromagnetic coupling among the three metals, as might have been expected for a monodentate carboxylate. Considering that iron– and manganese–carboxylates have been studied extensively, the fact that such simple, general reactions as those described here yield such structurally unexpected products suggests

(76) Blake, A. B.; Yavari, A.; Hatfield, W. E.; Sethulekshmi, C. N. *J. Chem. Soc., Dalton Trans.* **1985**, 2509.
(77) Gorun, S. M.; Papaefthymiou, G. C.; Frankel, R. B.; Lippard, S. J. *J. Am. Chem. Soc.* **1987**, *109*, 4244.
(78) Vef, A. MODEL2 *Fit and Evaluation Program Version 2.4*; Institut für Anorganische Chemie und Analytische Chemie, Johannes-Gutenberg Universität: Mainz, Germany, 1990.
(79) Reem, R. C.; Solomon, E. I. *J. Am. Chem. Soc.* **1987**, *109*, 1216.
(80) Gorun, S. M.; Lippard, S. J. *Inorg. Chem.* **1991**, *30*, 1625.
(81) Surerus, K. K.; Münck, E.; Snyder, B. S.; Holm, R. H. *J. Am. Chem. Soc.* **1989**, *111*, 5501.
(82) Snyder, B. S.; Patterson, G. S.; Abrahamson, A. J.; Holm, R. H. *J. Am. Chem. Soc.* **1989**, *111*, 5214.
(83) Münck, E.; Papaefthymiou, V.; Surerus, K. K.; Girerd, J.-J. *ACS Symp. Ser.* **1988**, *327*, Chapter 15.
(84) Borovik, A. S.; Hendrich, M. P.; Holman, T. R.; Münck, E.; Papaefthymiou, V.; Que, L., Jr. *J. Am. Chem. Soc.* **1990**, *112*, 6031.
(85) Hendrich, M. P.; Münck, E.; Fox, B. G.; Lipscomb, J. D. *J. Am. Chem. Soc.* **1990**, *112*, 5861.
(86) Christou, G., personal communication.
(87) Johnson, C. K. ORTEP-II, *A Fortran Thermal Ellipsoid Plot Program*; Report ORNL-5138, Oak Ridge National Laboratory: Oak Ridge, TN, 1976.

that there yet remains much chemistry to be explored in this area.

**Acknowledgment.** We are grateful to the National Institute of General Medical Sciences and the National Science Foundation for support of this research. Additional support was provided by the National Institutes of Health (Training Grant CA-09112, R.L.R.), the Deutscher Akademischer Austauschdienst (NATO Science Fellowship, P.P.), and the American Cancer Society (fellowship to W.B.T.). We thank Dr. G. C. Papaefthymiou for assistance in obtaining Mössbauer data at the Francis Bitter National Magnet Laboratory, which was supported by the National Science Foundation, and Dr. P. Nordlund for permission to quote his results prior to publication.

**Supplementary Material Available:** Tables of atomic coordinates, equivalent isotropic thermal parameters, anisotropic thermal parameters, bond distances and angles, and observed and calculated temperature-dependent magnetic susceptibilities for **1** and **2**, respectively, and the derivation of the temperature-dependent magnetic susceptibility equations for **1** and **2** (79 pages); tables of observed versus calculated structure factors (213 pages). Ordering information is given on any current masthead page.

# Steady-State and Time-Resolved Fluorescence Investigations of Pyrene Excimer Formation in Supercritical $CO_2$†

**JoAnn Zagrobelny, Thomas A. Betts, and Frank V. Bright***

*Contribution from the Department of Chemistry, Acheson Hall, State University of New York at Buffalo, Buffalo, New York 14214.* *Received October 18, 1991. Revised Manuscript Received March 4, 1992*

**Abstract:** Detailed studies on the formation of pyrene excimer in supercritical $CO_2$ are reported. The photophysics of pyrene are investigated as a function of temperature and fluid density. Over the broad density range studied, there is no evidence for ground-state (solute–solute) interaction. Comparison is made between excimer formation in supercritical $CO_2$ and ground-state dimerization of pyrene in $\gamma$-cyclodextrin ($\gamma$-CD). Time-resolved fluorescence spectrocopy is used to recover the individual rate terms that describe the total emission process. The recovered density-dependent bimolecular rates for pyrene excimer formation in supercritical $CO_2$ follow a simple diffusion-controlled model. This result parallels reports on pyrene excimer formation in normal liquid solvents. Finally, the relative decrease in pyrene excimer formation, with increased fluid density, is easily explained from our time-resolved experiments.

## Introduction

Many physicochemical properties describe a chemical substance or mixture. For example, the boiling point, density, and dielectric constant can all be used to characterize (at least partially) a particular species or system. If a substance is heated and maintained above its critical temperature, it becomes impossible to liquefy it with pressure.[1] Furthermore, when pressure is applied to this system, a single phase forms that exhibits unique physicochemical properties. This single phase is termed a supercritical fluid and is characterized by a critical temperature and pressure ($T_c$ and $P_c$, respectively).

Supercritical fluids are intriguing and offer a convenient means to adjust a solvent medium from gas- to liquid-like characteristics without actually changing the chemical structure of the medium. Moreover, by proper control of pressure and temperature one can survey a significant range of physicochemical properties (density, diffusivity, viscosity, dielectric constants, etc.) without ever passing through a phase boundary. That is, a supercritical fluid can be considered a continuously adjustable solvent.

As a consequence of their unique characteristics, supercritical fluids have received a great deal of attention in a number of important scientific fields.[1-14] Often there are many reasons given for choosing a supercritical fluid over another medium, but it turns out that that choice is governed typically by the following: (1) the ease with which the chemical potential can be varied simply by adjustment of the system pressure[13] and (2) the unique solvation and favorable mass transport properties.[5]

Over the past decade, much progress is supercritical fluid science and technology has occurred. For example, supercritical fluids have found widespread use in extractions,[2-5] chromatography,[6-9] chemical reaction processes,[10,11] and oil recovery.[12] Most recently, they have even been used as a solvent for carrying out enzyme-based reactions.[14] Unfortunately, although supercritical fluids are being used effectively in a myriad of areas, we still lack a detailed understanding of the fundamental processes that govern these peculiar solvents.

In an effort to overcome this disparity, significant effort has been devoted to determining the fundamental aspects of solute–solute, solute–fluid, and solute–cosolvent interactions in supercritical fluids.[15-45] The bulk of these efforts have used optical

* Author to whom all correspondence should be addressed.

† Dedicated to Professor Gary M. Hieftje on the occasion of his 50th birthday.

(1) Reid, R. C.; Prausnitz, J. M.; Poling, B. E. *The Properties of Gases and Liquids*, 4th ed.; McGraw-Hill: New York, 1987.
(2) McHugh, M. A.; Krukonis, V. J. *Supercritical Fluid Extraction-Principles and Practice*; Butterworths: Boston, MA, 1986.
(3) Paulaitis, M. E.; Krukonis, V. J.; Kurnik, R. T.; Reid, R. C. *Rev. Chem. Eng.* **1983**, *1*, 179.
(4) Paulaitis, M. E.; Kander, R. G.; DiAndreth, J. R. *Ber. Bunsen-Ges. Phys. Chem.* **1984**, *88*, 869.
(5) Brennecke, J. F.; Eckert, C. A. *AIChE J.* **1989**, *35*, 1409.
(6) Klesper, E. *Angew. Chem., Int. Ed. Engl.* **1978**, *17*, 738.
(7) Novotny, M. V.; Springston, S. R.; Peaden, P. A.; Fjeldsted, J. C.; Lee, M. L. *Anal. Chem.* **1981**, *53*, 407A.
(8) *Supercritical Fluid Chromatography*; Smith, R. M., Ed.; Royal Society of Chemistry Monograph: London, UK, 1988.
(9) Smith, R. D.; Wright, B. W.; Yonker, C. R. *Anal. Chem.* **1988**, *60*, 1323A.
(10) Brunner, G. *Ion. Exch. Solvent Extr.* **1988**, *10*, 105.
(11) Eckert, C. A.; Van Alsten, J. G. *Environ. Sci. Technol.* **1986**, *20*, 319.
(12) *Supercritical Fluids - Chemical Engineering Principles and Applications*; Squires, T. G., Paulaitis, M. E., Eds.; ACS Symposium Series 329; American Chemical Society: Washington, DC, 1987.
(13) van Wasen, U.; Swaid, I.; Schneider, G. M. *Angew. Chem., Int. Ed. Engl.* **1980**, *19*, 575.
(14) Aaltonen, O.; Rantakyla, M. *CHEMTECH* **1991**, *21*, 240.
(15) Eckert, C. A.; Ziger, D. H.; Johnston, K. P.; Ellison, T. K. *Fluid Phase Equilib.* **1983**, *14*, 167.
(16) Eckert, C. A.; Ziger, D. H.; Johnston, K. P.; Kim, S. *J. Phys. Chem.* **1986**, *90*, 2738.
(17) Kim, S.; Johnston, K. P. *Ind. Eng. Chem. Res.* **1987**, *26*, 1206.

0002-7863/92/1514-5249$03.00/0 